A finite element method for a weakly nonlinear dynamic analysis and bifurcation tracking of thermo-acoustic instability in longitudinal and annular combustors

A finite element method for a weakly nonlinear dynamic analysis of thermo-acoustic instability in longitudinal and annular combustors

D. Laera[a,*], G. Campa[b], S.M. Camporeale[a]

[a] *Politecnico di Bari, 70125 Via Re David, 200, Bari (Ba), Italy*
[b] *Product Development Turbomachinery and Combustion, Ansaldo Sviluppo Energia S.r.l, 16152, Genova, Italy*

Abstract

Low-frequency nonlinear dynamics of thermo-acoustic modes in longitudinal and annular combustors have been intensively studied experimentally, numerically, and theoretically to better understand the mechanisms leading to limit cycles. This article presents a numerical procedure based on a finite element method able to perform weakly nonlinear analysis of longitudinal as well as multi-burner annular combustors considering complex nonlinear flame models. At first the proposed numerical procedure is validated in a longitudinal configuration against analytical results obtained in a low-order framework, nonlinear flame models with a third-order and of a fifth-order polynomial with time delays are assumed. Subsequently, the ability of the proposed numerical approach to treat complex combustion systems with independent flames is verified on an annular configuration equipped with twelve burners. In both configurations, at the variation of the acoustic-combustion interaction index n, the amplitudes of velocity fluctuations of the predicted

*Corresponding author: davide.laera@poliba.it

limit cycles are plotted against the control parameter to track the bifurcation diagrams. Regardless of the configuration, supercritical and subcritical bifurcations are obtained depending of the chosen flame model. In a second step, the influence on the bifurcation trajectories of the time delay and of the amount of acoustic damping is investigated. Results reveal an influence of both parameters on the position of the Hopf bifurcation points and of the fold points and also an impact on the limit cycle amplitude of the velocity fluctuations.

Keywords: Thermo-acoustic instabilities, Helmholtz solver, Longitudinal combustor, Annular combustor, Limit cycles, Bifurcation diagrams

---

1. Introduction

Lean premixed combustors used in modern gas turbines for power generation and aero-engines are often affected by combustion instabilities generated by mutual interactions between pressure fluctuations (p') and heat release rate oscillations ($\dot{q}'$) produced by the flame [1, 2, 3]. Many theoretical and numerical studies are focused on the analysis of limit cycles of low-frequency instabilities considering simple longitudinal configurations assuming theoretical flame response models [4, 5, 6, 7]. The main difficulty to perform these analyses is the definition of the model used to describe the response of the flame to acoustic perturbations [8]. If a linear response is assumed, a stability analysis can be performed in order to identify the frequency at which the system is unstable meaning that pressure oscillations may start after infinitesimally small disturbances [9, 10, 11, 12]. However, linear tools cannot account for finite amplitude effects on the oscillation frequency and cannot predict the fluctuations level. These features can be examined by combining an acoustic model of the system with a nonlinear description of the flame dynamics [13, 7]. The evaluation of a suitable nonlinear flame model for a given combustor is, probably, one of the most challenging task of the study of thermo-acoustic combustion instability. In annular configurations more difficulties arise due to the presence of multiple flames which respond collectively over a wide frequency range [14]. The present study deals with these difficulties developing a numerical approach able to perform limit cycle calculations considering complex nonlinear flame models with time delays in combination with a Helmholtz solver, using this framework to calculate the limit cycle conditions and the bifurcation diagrams of a single burner longitudinal combustor and of a more complex multi-burner annular configuration.

At this point, it is worth briefly reviewing some recent investigations of nonlinear flame models. First studies on the transition to the limit cycle were carried out in solid fuel rocket motors by Culick who observed that some stable motors would suddenly jump to a self-sustained oscillation state, when pulsed [15]. Since in rocket engines the oscillations have such high amplitudes that the gas dynamics is nonlinear, he considered nonlinear gas dynamics and linear flame models. Nonlinear combustion models were later taken into account [16], assuming that the heat release rate was a quadratic or rectified (modulus sign) function of the fluctuating velocity or pressure.

The bifurcation diagram can be helpful for understanding the influence of nonlinear flame model, since it shows the amplitude of limit cycles as a function of control parameters. This is useful if there is a known bound on the acceptable oscillation amplitude. It also shows whether the point of linear instability (the so called Hopf bifurcation point) is supercritical or subcritical. This is an important qualitative distinction because: in a subcritical system, high amplitude oscillations occur suddenly when the state becomes linearly unstable and even when the system is linearly stable; in a supercritical system, amplitude oscillations occur only when the system is linearly unstable [17].

In the years several techniques have been proposed in order to track the bifurcation diagrams. Due to the complexity of the problem most of them deals with longitudinal combustor characterized by one single source of heat release rate. Subcritical bifurcation is obtained by Moeck *et al.* [18] performing a systematic variation of parameters and tracking direct time integration. However this method is computationally expensive.

Another method for obtaining the bifurcation diagrams is numerical continuation [16, 19, 20]. This approach is based on the iterative solution of a set of parameterized nonlinear equations given an initial guess. The diagram is tracked varying a parameter and including the solutions which satisfy the set of equations for a given state of the system. The unstable limit cycle can also be computed. Compared to other methods, it is very efficient in obtaining the dependence of the solution from the control parameter. However, it takes a long time to map the bifurcation diagram and it can be also too computationally expensive. Thanks to improvements in the method and in the parallel computing, continuation methods are likely to become important tools in nonlinear analysis of thermo-acoustics [21].

Juniper [21] and Subramanian *et al.* [22] used DDE-BIFTOOL, which is a software based on the numerical continuation methods for delay systems [23].

The steady state of the system is evaluated through the Newton-Raphson scheme and the steady state solution is used for tracking the bifurcation diagram as the control parameter varies. The use of low-order network models to map the bifurcation diagram as a function of a control parameter has been shown by Campa and Juniper [24]. Instead of numerically integrate the fully non-linear equations governing the phenomenon, the authors proposed a weakly nonlinear approach consisting in a linear eigenvalue analysis around a non-linear steady state of the system. This approach, less computationally expensive than the continuation method, will be used in this work. Subramanian *et al.* [5] has analyzed subcritical transition to instability relating the non-linearity in the model with the criticality of the ensuing bifurcation, starting from the equation of Stuart-Landau. They also identify the parameter regions where triggering is possible using the method of harmonic balance.

The Flame Describing Function (FDF) approach was developed to reproduce the limit cycles experimentally observed [25]. The stability map of a burner with an unconfined flame [26] and of a burner with a confined flame [27, 28] was obtained by using flame describing functions. Recently this methodology was applied to the case of turbulent premixed swirled flames [7, 29]. Additionally, a diffusion flame characterizing a Rijke tube has been modeled by means of flame describing function to get the stability map [30]. Nonlinear effects induced by nonstandard types of fluctuations in a multiple flame combustor equipped with a perforated plate were investigated by Kabiraj *et al.* [31]. Very recently, Heckl [32] has modeled the measured Flame Describing Function by Noiray *et al.* [26] with an entirely analytical approach, finding the pattern of the oscillation regimes in parameter space, such as frequency and amplitude of limit cycles at different conditions. However, it should be notice that a FDF does not provide only the flame response of a specific combustor but is also a description of the entire burner area, including the effects of flame confinement, heat losses and interaction of the flame with the walls, all aspects that make the FDF linked to the specific combustor and operating conditions at which the measurements are performed.

Very few are the works in which a nonlinear analysis is performed on an annular combustor. The problem may be simplified by considering only one single azimuthal mode described by Van der Pol oscillator equations coupled with a nonlinear flame model expressed in terms of pressure perturbation. Results in [33, 34, 35] indicate that this approach is able to predict both spinning and standing unstable modes depending on the nonlinearity and nonuniformity in the flame response. Recently, Bourgouin *et al.* [36] managed to introduce in their analytical one-dimensional framework a more reliable experimental Flame Describing Function (FDF) however the heat release rate from the different burners is considered uniformly distributed over the circumference of the annular chamber. Following this approach, the spinning instability recorded during experiments of the laboratory scale MICCA annular combustor was reproduced in terms of frequency and amplitude of velocity fluctuations at the limit cycle. Multiple independent flames are considered in the acoustic network modeling approach developed by Parmentier *et al.* [37] followed by Bauerheim *et al.* [38]. They presented however, only a linear stability analysis of spinning and standing modes assuming a simple time delay n-τ dynamical response. Three dimensional geometries may be analyzed by means a Helmholtz solver approach. In the time domain Pankiewitz and Sattelmayer [39], examined a three-dimensional combustion chamber, predicting the amplitude of limit cycles determined by a nonlinear flame model with a very simple saturation mechanism. Campa and Camporeale [10, 40] performed a linear stability analysis of a practical annular combustor assuming a distributed flame transfer function. On the computational level, Large-Eddy Simulation (LES) codes have been used to investigate combustion instability by suitably calculating pressure oscillations in combination with turbulent combustion phenomena [41, 42]. Large numerical resources are, however, required.

The present article specifically reports a numerical technique able to perform a weakly nonlinear analysis of thermo-acoustic combustion instabilities in a Helmholtz solver framework. In the frequency domain, the limit cycle condition, i.e. the condition in which the growth rate α equals zero, is predicted solving the damped inhomogeneous Helmholtz equation coupled with two theoretical nonlinear flame models derived multiplying a linear n-τ flame transfer function (FTF) with a third-order and fifth-order polynomial expression which saturate the gain of the FTF with the increase of the amplitude of velocity fluctuations $|\hat{u}/\overline{u}|$. At first the analysis is performed on a longitudinal combustor. Varying the acoustic-combustion interaction index n, the bifurcation diagrams are tracked assuming both nonlinear flame models. In a second step, for the first time, the analysis is conducted in an annular combustor with indipendent flames proving the feasibility of the presented numerical approach also for multiple flames configurations. In both configurations, the influence on the predicted limit cycles of the time delays and of the damping level considered in the systems is also investigated. The article is organized as follow. After an overview of the nonlinear analysis theory presented in Section 2, the thermo-acoustic theory and the description of the flame models used in the study are presented in Section 3. Results are discussed in Section 4 for both configurations analyzed.

2. Nonlinear analysis

The behaviour of a nonlinear unstable system can change as a control parameter varies. These qualitative changes in the system dynamics are called bifurcations and the parameter values at which they occur is called bifurcation point [17].

Figure 1 shows two diagrams, describing the bifurcation dynamics as a function of a control parameter R. The variable on the y-axis is the steady state amplitude of the system, which is the limit cycle amplitude. At low values of R the system tends to a zero amplitude stable solution (solid line in Fig. 1). When R reaches the Hopf bifurcation point, the solution of the system becomes unstable. Increasing the value of the control parameter, the solution at zero amplitude remains unstable (dashed line in Fig. 1) and the system starts to oscillate reaching the steady state amplitude (solid line at non-zero amplitudes), known as the limit cycle or the stable periodic solution.

The nonlinear behavior around the Hopf bifurcation point determines two different types of bifurcation and how the system answers to nonlinear perturbations. The first type is the supercritical bifurcation (Fig. 1a), which is characterized by a gradually increase of the amplitude once reached the

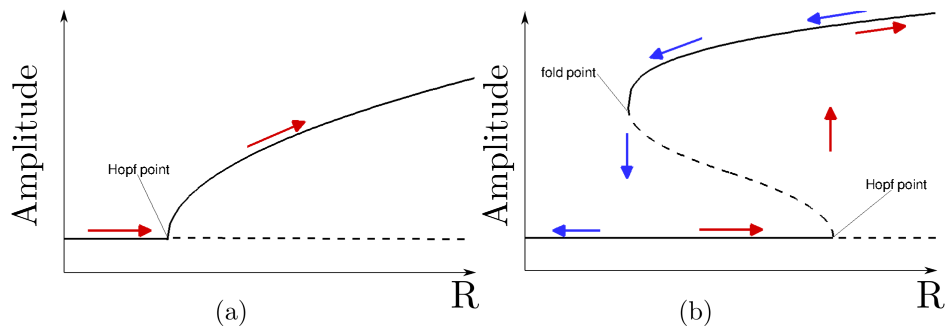

Figure 1: Steady state oscillation amplitude as a function of R for (a) a supercritical bifurcation and (b) a subcritical bifurcation [24]. As the control parameter R is increased, the system follows the red arrow path. As it is decreased, the system follows the blue arrow path.

Hopf point. In this condition, all perturbations imposed on the system tend to decay to zero only if the Hopf point is not reached, otherwise all the perturbations reach a new stable periodic solution at the limit cycle equilibrium. The second type of behavior is the subcritical bifurcation (Fig. 1b), which is characterized by a sudden increase of the steady state amplitude at the Hopf point. Once reached the limit cycle equilibrium, the perturbations imposed on the system continue to reach a stable periodic solution even for values of R lower than the one corresponding to the Hopf point, until the fold point is reached. For values of R lower than the one corresponding to the fold point, all perturbations decay to zero, as shown by the blue arrow path in Fig. 1b. The dashed line at non-zero amplitudes in Fig. 1b is known as the unstable periodic solution [17]. If the system is triggered to an amplitude below the unstable periodic solution, the imposed perturbations tend to decay to zero. Otherwise, the imposed perturbations tend to grow reaching the stable periodic solution.

Considering the condition of a subcritical bifurcation as in Fig. 1b, the behaviour of the growth rate as a function of the amplitude for a generic value of the control parameter in the bi-stable zone is shown in Fig. 2. As well described by Strogatz [17], two fixed points can be observed referring to periodic solutions: the fixed point indicated with a full point refers to a stable periodic solution, the fixed point indicated with a hollow point refers to an unstable periodic solution. It can also be observed that if the derivative of the growth rate to the amplitude at a constant control parameter is positive, the fixed point is an unstable periodic solution. If the derivative of the growth rate to the amplitude at a constant control parameter is negative, the fixed point is a stable periodic solution.

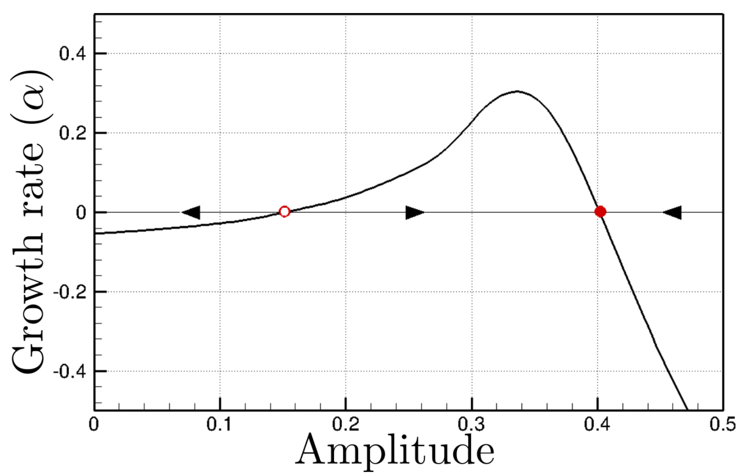

Figure 2: Growth rate (α) as a function of the amplitude for a generic value of the control parameter in the bistable zone, when a subcritical bifurcation occurs.

3. The thermo-acoustic problem: Helmholtz solver approach

The derivation of the mathematical model used for thermo-acoustic studies will be briefly discussed in this section. The complete formulation can be found in other works [12, 43].

The fluid is regarded as an ideal gas. The effects of viscosity, thermal diffusivity and heat transfer with walls are neglected, the mean pressure is assumed uniform in the domain. The mean flow velocity $\overline{u}$ is assumed much lower than the speed of sound (hypothesis that is generally verified in the combustion chamber of gas turbines [2]), so its influence on the propagation of the pressure waves inside the duct is negligible. Under such hypotheses, in presence of heat fluctuations, the inhomogeneous wave equation can be obtained [12]

$$\frac{1}{\overline{c}^2}\frac{\partial^2 p'}{\partial t^2} - \overline{\rho}\nabla \cdot \left(\frac{1}{\overline{\rho}}\nabla p'\right) = \frac{\gamma - 1}{\overline{c}^2}\frac{\partial \dot{q}'}{\partial t}, \tag{1}$$

where p' is the pressure fluctuation, $\dot{q}'$ is the heat release rate fluctuation per unit volume, γ is the ratio of specific heats, ρ is the density and c is the speed of sound. The effects of losses due to viscous and thermal boundary layers can be modelled making use of suitable acoustic impedance as boundary conditions. Here, aiming at analyzing the effects of damping, for one dimensional combustion systems, the first derivative of p' in Eq. (1) is multiplied by a nondimensional damping coefficient ζ [44], giving

$$\frac{1}{\overline{c}^2}\frac{\partial^2 p'}{\partial t^2} + \frac{\zeta}{c\mathcal{L}}\frac{\partial p'}{\partial t} - \overline{\rho}\nabla \cdot \left(\frac{1}{\overline{\rho}}\nabla p'\right) = \frac{\gamma - 1}{\overline{c}^2}\frac{\partial \dot{q}'}{\partial t}, \tag{2}$$

where $\mathcal{L}$ is the characteristic dimension of the analysed system. In this work, $\mathcal{L}$ is assumed equal to the radius in the longitudinal configuration and to $\sqrt{R_{ex}^2 - R_{in}^2}$ in case of the annular combustor, being R_{ex} and R_{in}, respectively, the external and the internal radius of the annulus domain in which ζ is considered. The damping coefficient for j^{th} mode is modelled as

$$\zeta_j = c_1 j^2 + c_2 j^{1/2} \tag{3}$$

where c_1 and c_2 are assumed constant for each mode. In this study, the damping coefficients ζ is varied from 0.03 to 0.3. More information on these coefficients can be found in [45]. This is the only damping mechanism considered in this study. In all configurations analysed, either p' or u' are set to zero at the boundaries of the computational domain, so that the energy acoustic flux (f=$p'\mathbf{u}'$) through the boundaries is null [43].

In the present article, the thermo-acoustic problem is solved in the frequency domain. The fluctuating variables are expressed by complex functions of time and position with a sinusoidal form: p'=$\Re(\hat{p}\exp(i\omega t))$, where ω is a angular frequency. Applying the harmonic analysis for p' and $\dot{q}'$ in Eq. (2) the damped inhomogeneous Helmholtz equation is obtained in the frequency domain

$$\frac{\lambda^2}{\overline{c}^2}\hat{p} - \frac{\lambda\zeta}{c\mathcal{L}}\hat{p} - \overline{\rho}\nabla \cdot \left(\frac{1}{\overline{\rho}}\nabla\hat{p}\right) = -\frac{\gamma - 1}{\overline{c}^2}\lambda\hat{\dot{q}} \tag{4}$$

where $\lambda = -i\omega$. With the definition of the flame model, Eq. (4) yields a classical linear stability problem at the eigenvalues λ [17]. In the eigenvalue problem, ω is a complex angular frequency, its real part gives the frequency of the oscillations, f=$\Re(\omega)/2\pi$ Hz, while the imaginary part of ω corresponds to the growth rate α=$-\Im(\omega)/2\pi$ s^{-1} parameter that governs the stability the system, considering that the damping is directly model in the solved equations. If α is positive, the acoustic mode is unstable so the amplitude of fluctuations grows with time. If α is negative, the acoustic mode is stable, i.e., perturbations decay with time. A limit cycle condition is reached when α=0.

3.1. The linear flame model

In the frequency domain, the linear flame model is assumed as the classical n-τ model [2, 46]

$$\frac{\hat{\dot{q}}}{\bar{\dot{q}}} = -n\frac{\hat{u}_i}{\overline{u}_i}\exp(-i\omega_r\tau), \tag{5}$$

where n is the acoustic-combustion interaction index, τ the time delay between the velocity fluctuations in a reference point $\hat{u}_i$ and the heat release rate fluctuations $\hat{\dot{q}}$. The minus sign derives by the definition of the n-τ model in terms of fluctuations of equivalence ratio $\hat{\phi}/\overline{\phi}$=$-\hat{u}/\overline{u}$ [47]. In order to examine only the phase shift induced by the flame and considering that always time delays smaller than the period of the analysed mode are assumed only the real part (ω_r) of the angular frequency ω is considered in the flame model of Eq. (5). The FTFs so modelled can be directly compared with the measured FTFs that are also defined in terms of the frequency of ω_r of the forcing signal used to measure the flame response [48].

3.2. The nonlinear flame models

Following Dowling [13], a theoretical nonlinear flame model is expressed as the product of the linear flame transfer function ($\mathcal{T}_L(\omega_r)$) shown in Eq. (5), which depends only on frequency, by another function that depends only on the amplitude of velocity fluctuations taken at the same reference point i

defined in Eq. (5)[1]. This function is referred as *Nonlinear Flame Transfer Function* NFTF($|\hat{u}/\overline{u}|$) [24, 49] and introduce a saturation of the gain G of the FTF with the increase of the amplitude of velocity fluctuations $|\hat{u}/\overline{u}|$. Under these assumptions, the analytical frame describing function becomes

$$\mathcal{T}^{NL}_{flame}(\omega_r, |\hat{u}/\overline{u}|) = \mathcal{T}_L(\omega_r) \cdot \mathrm{NFTF}(|\hat{u}/\overline{u}|). \tag{6}$$

The NFTF function derives directly from the nonlinearity introduced into the flame model and it can be computed taking the first order of the Fourier transform of the flame model formulated in the time domain (more details can be found in the Appendix 1). Hereafter are reported the NFTF functions for two flame models used in this study in which the heat release rate fluctuations are related to the velocity fluctuations through a third-order and a fifth-order polynomial law. In both cases, only the influence of the odd-powered polynomial terms are examined because, although even-powered polynomial terms are physically admissible, their contribution to the acoustic energy integrates to zero over a cycle, as can be observed in Appendix 1. The nonlinear flame model in which the third-powered term is the highest order is

$$\frac{\dot{q}'(t)}{\bar{\dot{q}}} = -n\left[\mu_2\left(\frac{u'(t-\tau)}{\overline{u}}\right)^3 + \mu_0\frac{u'(t-\tau)}{\overline{u}}\right], \tag{7}$$

where the coefficient μ_0 is chosen equal to unity noting that for $|\hat{u}/\overline{u}| \rightarrow 0$ the nonlinear flame model should tends to the linear model. The coefficient μ_2 is negative and its value is related to the effects of saturation of the flame

[1]In the remaining part of the article the subscript i will be omitted to improved the readability of equations.

response with large velocity fluctuations that are observed [44]. A parametric system identification technique based on engine data can be used, as proposed by Noiray *et al.* [35], in order to evaluate the third-order polynomial flame model. In this study μ_2=-2. The function NFTF for this model (algebraic steps are shown in the Appendix 1) results

$$\mathrm{NFTF} = \frac{3}{4}\mu_2|\hat{u}/\overline{u}|^2 + \mu_0. \tag{8}$$

The pattern of the NFTF function of Eq. (7) is shown in Fig. 3. Only positive values of the amplitude $|\hat{u}/\overline{u}|$ are considered to ensure the physical meaning of the flame model. It is possible to observe that the NFTF manifests a monotone decreasing pattern for increasing amplitudes until zero is reached for $|\hat{u}/\overline{u}|$=0.81. The NFTF is assumed null also for higher values of amplitude of velocity fluctuations.

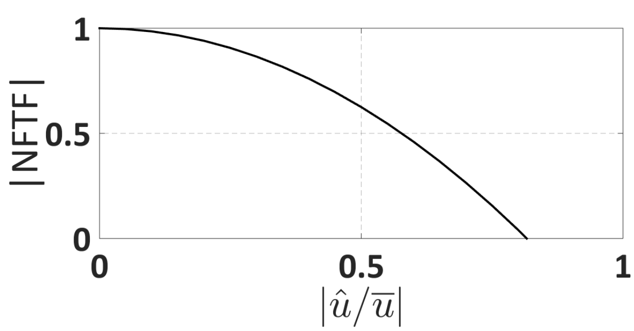

Figure 3: Pattern of the NFTF function for the third-order polynomial flame model of Eq. (7) with μ_0=1 and μ_2=-2.

The nonlinear flame model in which the fifth-powered term is the highest order is

$$\frac{\dot{q}'(t)}{\bar{\dot{q}}} = -n\left[\mu_4\left(\frac{u'(t-\tau)}{\overline{u}}\right)^5 + \mu_2\left(\frac{u'(t-\tau)}{\overline{u}}\right)^3 + \mu_0\frac{u'(t-\tau)}{\overline{u}}\right], \tag{9}$$

where μ_4, μ_2 and μ_0 are coefficients equal to -5, 5 and 1, respectively. The function NFTF for this model (see Appendix 1) is

$$\mathrm{NFTF} = \frac{5}{8}\mu_4|\hat{u}/\overline{u}|^4 + \frac{3}{4}\mu_2|\hat{u}/\overline{u}|^2 + \mu_0. \tag{10}$$

The pattern of the NFTF function of Eq. (7) is shown in Fig. 4. Differently from the previous case shown in Fig. 3 the function has an initial increase reaching its maximum value, after which it decreases until zero is reached at $|\hat{u}/\overline{u}|$=1.19.

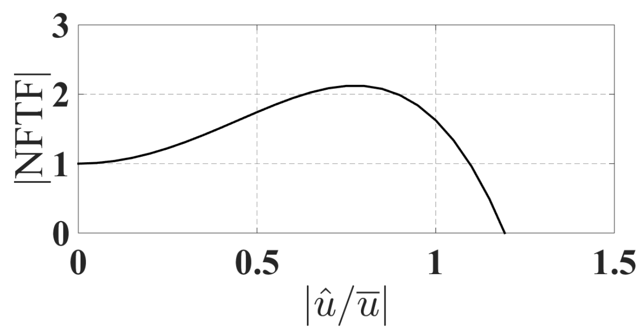

Figure 4: Patterns of the NFTF function for the fifth-order polynomial flame model of Eq. (9) with μ_0=1, μ_2=5 and μ_4=-5.

3.3. Linear and weakly nonlinear stability analysis

The numerical analysis is carried out by using the finite element method (FEM) based the commercial software *Comsol Multiphysics*. This code solves the classical Helmholtz equation in which the heat release rate fluctuations are treated as pressure source. In order to include the damping, the second term of the Eq. (2) ($-\lambda\zeta/\overline{c}\mathcal{L}\hat{p}$) is considered on the RHS of the equation together with the heat release rate fluctuations

$$\begin{cases} \dfrac{\lambda^2}{\overline{c}^2}\hat{p} - \overline{\rho}\nabla \cdot \left(\dfrac{1}{\overline{\rho}}\ \nabla\hat{p}\right) = -\dfrac{\gamma-1}{\overline{c}^2}\lambda\hat{\dot{q}} + \dfrac{\lambda\zeta}{\overline{c}\mathcal{L}}\hat{p} & (11) \\ \hat{\dot{q}} = \bar{\dot{q}}\dfrac{\hat{u}}{\overline{u}}\mathrm{NFTF}e^{-i\omega_r\tau} & (12) \\ i\omega\hat{u} + \dfrac{1}{\overline{\rho}}\nabla\hat{p} = 0 & (13) \end{cases}$$

The finite element discretization of this set of equations along with the boundary conditions results to the following eigenvalue problem [9]

$$[A]\,\mathbf{P} + \omega\,[B(\omega)]\,\mathbf{P} + \omega^2\,[C]\,\mathbf{P} = [D(\omega)]\,\mathbf{P}, \tag{14}$$

where $\mathbf{P}$ is the pressure eigenmodes vector, the matrices $[A]$ and $[C]$ contain coefficients originating from the discretization of the Helmholtz equation, $[B(\omega)]$ is the matrix of the boundary conditions and of the damping and $[D(\omega)]$ represents source term due to the unsteady heat release rate. In case of a linear stability analysis, i.e., assuming $|\hat{u}/\overline{u}| \rightarrow 0$, the NFTF equals unity and Eq. (12) can be directly used to model the heat release rate fluctuations in Eq. (11). However, with the introduction of the heat release the eigenvalue problem of Eq. (14) becomes nonlinear and is solved with an iterative algorithm. At the k^{th} iteration equation (14) is first reduced to a linear eigenvalue problem around a specific frequency Ω_k

$$([A] + \Omega_k\,[B(\Omega_k)] - [D(\Omega_k)])\,\mathbf{P} + \omega_k^2\,[C]\,\mathbf{P} = 0, \tag{15}$$

where $\Omega_k = \omega_{k-1}$ is the previous iteration result. The software uses the *ARPACK* numerical routine for large-scale eigenvalue problems. This is based on a variant of the Arnoldi algorithm, called the implicit restarted

Arnoldi method [50]. This procedure is iterated until the error defined by $\epsilon = |\omega_k - \Omega_k|$ is lower than a specific value, typically 10^{-6}.

For finite value of velocity fluctuations, the NFTF of Eq. (12) depends on the value of $|\hat{u}/\overline{u}|$. As already shown in previous works [7, 29] the weakly nonlinear approach allows to couple a linear tool, i.e., the eigenvalue analysis, with a nonlinear function linearizing the nonlinear term. This is obtained performing the eigenvalue analysis assuming an initial guess for the value of velocity fluctuations $|\hat{u}/\overline{u}|$ and reiterating this analysis increasing $|\hat{u}/\overline{u}|$ until the limit cycle condition, i.e., α=0 condition, is reached. For the calculation of the bifurcation diagrams, this numerical procedure is performed for each value of the acoustic-combustion interaction index n.

4. Results and discussion

The nonlinear behaviour of the flame modes of the third-order polynomial and fifth-order polynomial will be investigated. Two different configurations are examined: a longitudinal combustor with a single heat release zone and an annular combustor with multiple burners.

4.1. The longitudinal combustor

The first configuration analysed is a simple longitudinal combustor with a compact flame located in a narrow domain at around one quarter of the tube length, which is 3 m [10, 12]. Figure 5 shows the computational mesh and the location of the heat release is highlighted. The temperature increases from 300 K to 700 K across the combustion zone. An open condition, p'=0, is assumed at the inlet section and outlet section of the domain.

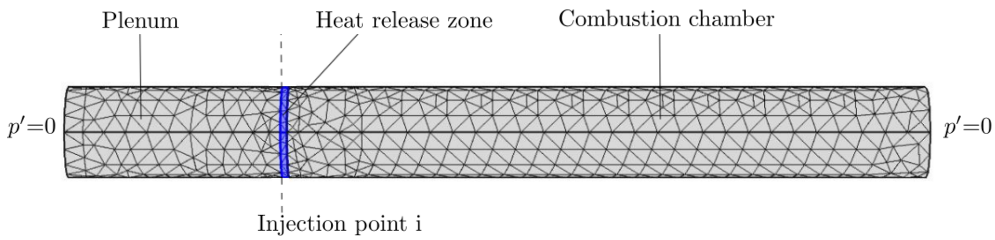

Figure 5: Computational mesh of the longitudinal combustor. The flame location is highlighted in blue.

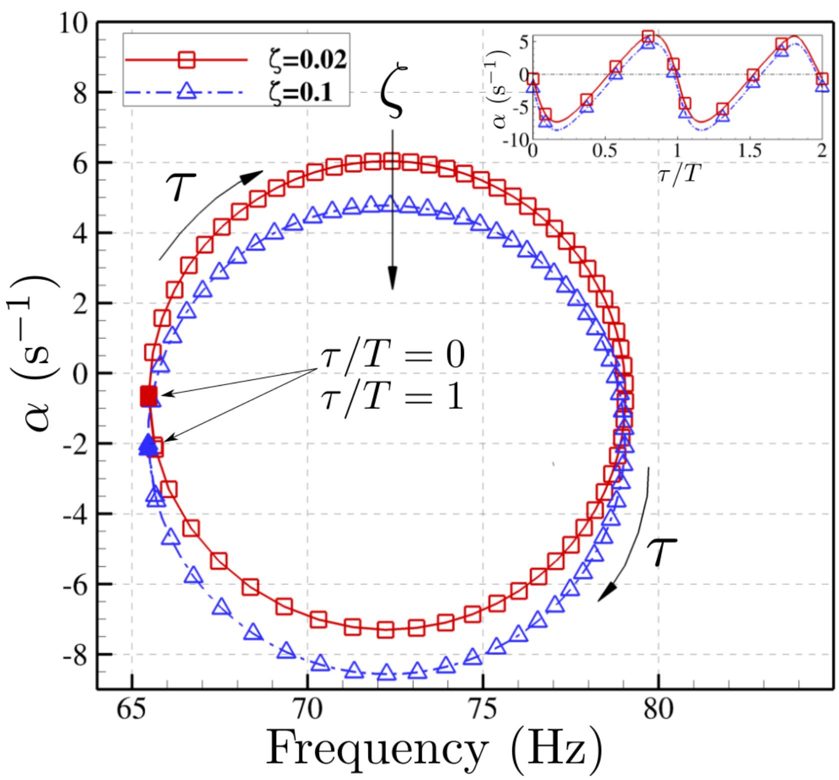

Figure 6: Frequency and growth rate (α) of the first eigenmode of the longitudinal combustor considering the flame model of Eq. (6) under the hypothesis of $|\hat{u}/\overline{u}| \rightarrow 0$.

At first, under the assumption of $|\hat{u}/\overline{u}| \rightarrow 0$, a linear stability analysis is performed considering the linear flame transfer function expressed in Eq. (5).

Considering the compactness of the flame, the time delay τ is assumed constant in the flame model. This analysis is useful to have a better comprehension of the influence on the system of the time delay and of the damping. In Fig. 6, the growth rate (α) is plotted against the frequency for the first axial mode of the system for different values of time delay τ, which is expressed normalized against the period of the mode T. The time delay τ is varied in order to keep τ/T from 0 to 1. The patterns are tracked for two values of the damping coefficient: ζ equal to 0.02 and 0.1. The acoustic-combustion interaction index n is kept equal to unity for this analysis. Figure 6 shows that frequency and growth rate decrease or increase depending on the value of the time delay assumed. Circular patterns like the ones found in [7] are found. This result is due to the chosen FTF where only the real part of the frequency is considered. Increasing the damping coefficient results in a vertical shift of the patterns towards more stable condition, i.e., growth rates decrease. The frequencies remain constant (frequency shifts are under 1 Hz). This is justified remembering that the frequency variation depends on the ratio between α/ω_r. If $\alpha/\omega_r \ll 1$ the complex frequency $\omega \sim \omega_r$ [51]. It should be notice that for the analysed condition this ratio is always far below the unity, e.g., in the condition where the absolute value of α is maximum $\alpha/frequency \sim 8/75 \sim 0.07$.

When a finite level of velocity fluctuations is considered in the model, a harmonic base weakly nonlinear stability analysis is performed and the bifurcation diagrams are mapped considering the acoustic-combustion interaction index n as the control parameter. Figure 8 shows the bifurcation diagram when the nonlinear flame model of Eq. (8), in which the third-powered term is the highest order, is introduced. A supercritical bifurcation is observed. The influence of the damping coefficient ζ and the time delay τ is examined and results are reported in Fig. 8a and Fig. 8b, respectively. In both diagrams, the rectangular marks indicate the position of the Hopf bifurcation point. For a fixed value of time delay equal to 11 ms (τ/T=0.78), the damping coefficient ζ is varied from 0 to 0.3. The black dashed line in Fig. 8a corresponds to the zero-damping condition, i.e., ζ=0. It is possible to observe that the system is unstable for any value of the control parameter n except for the condition with n=0. Furthermore, the amplitude of the limit cycle is constant and corresponds to the value that saturates the gain of the nonlinear flame model (the NFTF function) and nullifies the heat release rate fluctuations, as it is possible to observer in Fig. 8. For the specific case, this value of $|\hat{u}/\overline{u}|$ is equal to 0.81. When considering ζ non-zero, the position of the Hopf point moves towards higher values of the control parameter n as the damping level increases. For higher value of the acoustic-combustion interaction index, the increase of the energy dissipation rate causes a reduction of the amplitude of oscillations. However, due to the nonlinear saturation of the heat release rate, regardless the damping level, the amplitude $|\hat{u}/\overline{u}|$ tends asymptotically to the value, which saturates the heat release rate. In Fig. 8b for a fixed value of ζ=0.1 the time delay is varied from 8 ms to 13 ms. Starting from the condition in which the maximum amplitude of velocity fluctuation is registered, i.e., τ=11 ms, which corresponds to the more unstable condition in the linear stability analysis, an increase or decrease of the time delay produces a shift of the transition point at higher levels of the coefficient n and a decrease of the amplitude of velocity fluctuation for a given value of n.

Table 1 summarize the values of the frequencies in the Hopf point (f_{Hopf}). As shown in Fig. 6 the damping has small influence in the frequency, which varies only with the time delay τ. In particular, starting from the condition with the time delay equal to 8 ms, a reduction of the frequency is registered increasing τ. Figure 7 shows the wave shape of the resonant mode in the condition with τ=11 ms.

Table 1: Frequencies at the Hopf point (f_{Hopf}) for the nonlinear flame model of Eq. (7) for different time delays τ. Time delays are expressed in milliseconds. Frequencies in Hertz (Hz).

	τ=8	τ=9	τ=10	τ=11	τ=12	τ=13
f_{Hopf}	74.8	73.6	72.7	71.5	69.5	66

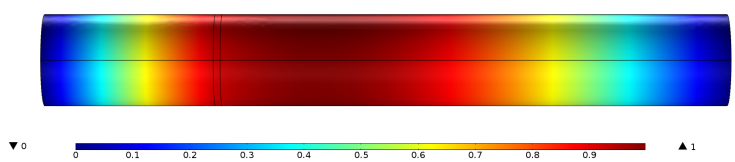

Figure 7: Normalized absolute pressure of the first longitudinal mode of the combustion chamber considering a time delay equal to 11 ms.

A different behaviour is registered when the nonlinear flame model of Eq. 9, in which the fifth-power term is the highest order, is introduced into the model. In this case, the system undergoes a subcritical bifurcation as is shown in Fig. 9. The continuous black lines indicate the stable branch of the diagram, while the unstable branch is reported with dashed lines. Both the Hopf bifurcation point and the fold bifurcation point are indicated with

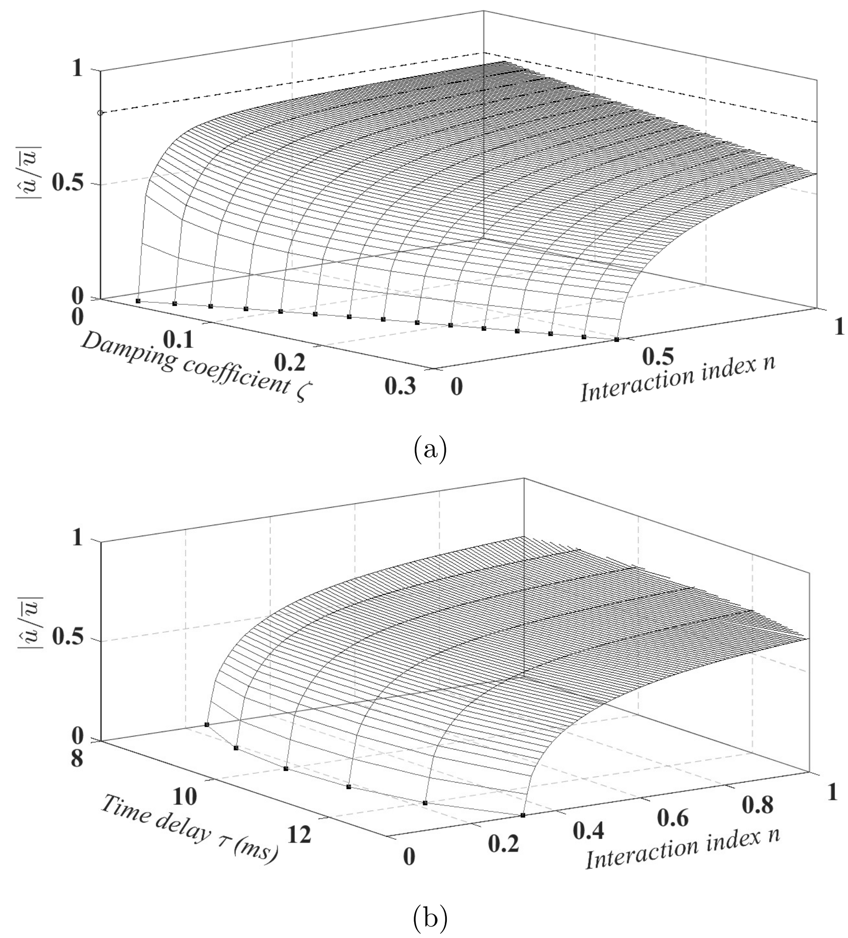

Figure 8: Bifurcation surfaces when the nonlinear flame model of Eq. (7) is considered. (a) influence of the damping coefficient ζ with a time delay τ=11 ms; (b) influence of the time delay τ with ζ=0.1.

rectangular marks. Starting from the Hopf bifurcation point, the proposed numerical technique is able to converge also in the unstable zone of the diagram. Also for this case a sensitivity analysis to the damping coefficient ζ and the time delay τ is performed. Similar to the previous case, in Fig. 9a for a fixed value of time delay of 11 ms, the damping coefficient ζ is varied from zero to 0.3. If no damping is considered, the system results always unstable except for the case with n=0 (dashed line in Fig. 9a). Differently from the previous flame model, the saturation of the NFTF function occurs at a higher amplitude value equals to 1.19 as it is possible to observe from Fig. 4. Increasing the damping level results in a shift towards higher values of the control parameter n of both the Hopf bifurcation point and the fold point. On the contrary, the velocity amplitude $|\hat{u}/\overline{u}|$ corresponding to the fold bifurcation point is not influenced by the level of the damping. This behaviour is typical of systems that manifest a subcritical bifurcation as shown in Subramanian *et al.* [5] where similar results are found for a different flame model and with a different methodology. As noticed with the first nonlinear flame model, the amplitude of the stable limit cycle solution tends to be the same for all the cases at high values of n. In Fig. 9b for a fixed value of ζ=0.1 the time delay is varied from 8 ms to 13 ms. Again, starting from the more unstable condition at τ=11 ms, a variation of the time delay induces a shift of the Hopf point and the fold point towards higher level of n. The amplitude of the fold bifurcations remains constant.

To verify these results, the two flame models of Eq. (7) and Eq. (9) are considered in the Low-order code "OSCILOS" [52]. Only the bifurcations diagrams with ζ=0.1 and τ=11 ms are computed in the analytic framework assuming similar for the other configurations. Since in the low-order code the acoustic waves are modelled as 1-D plane waves without the possibility to add the damping term of Eq.(11), the eigenvalue procedure is reiterated for different amplitude levels starting from $|\hat{u}/\overline{u}|$=0 and incrementing this value until a limit cycle condition which is reached when α=δ with the damping

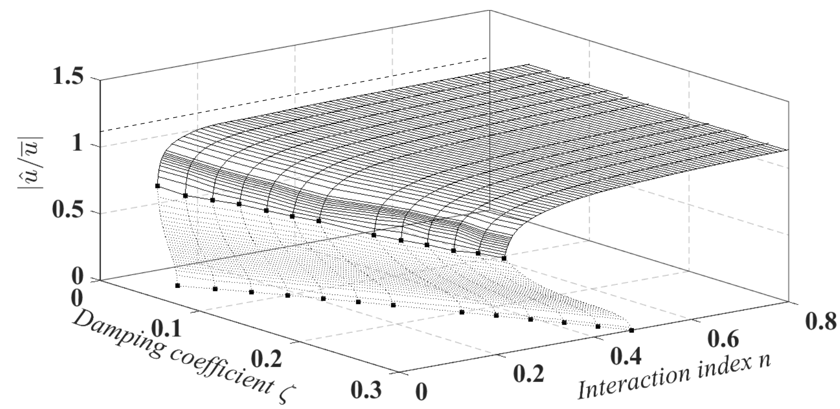

(a)

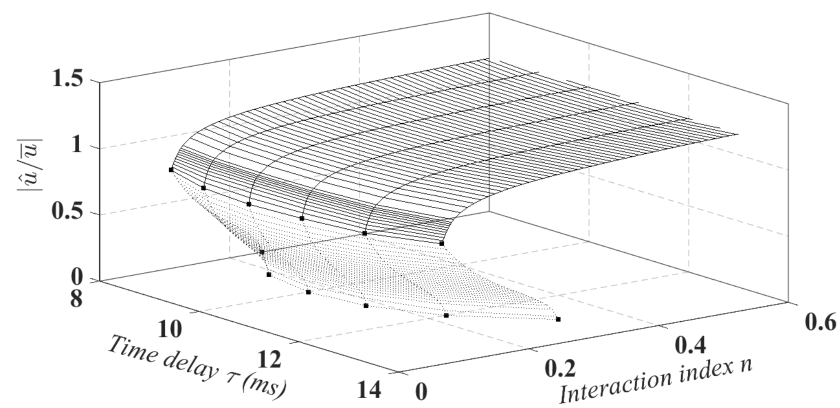

(b)

Figure 9: Bifurcation surfaces when the nonlinear flame model of Eq. (9) is considered. (a) influence of the damping coefficient ζ with time delay τ=11 ms; (b) influence of the time delay τ with a damping coefficient ζ=0.1.

rate δ=2.22 s^{-1} computed by means of simulations in the Helmholtz solver under "passive flame" conditions, i.e., considering only the steady combustion process with $\hat{\dot{q}}$=0 in Eq. (11). Figure 10 shows that there is a perfect overlap between the analytical results and the results of the Helmholtz solver calculations, for the supercritical and the subcritical case.

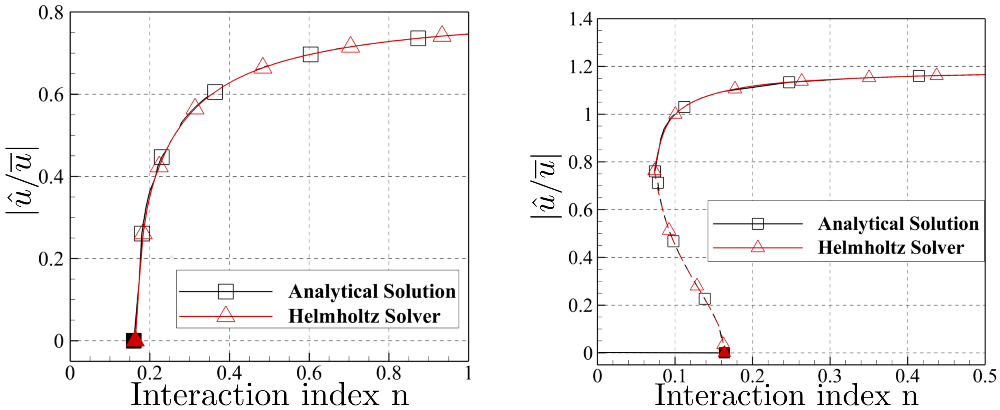

(a) (b)

Figure 10: Comparison between the supercritical (a) and subcritical (b) bifurcation diagrams assuming τ=11 ms and ζ=0.1 computed with the Helmholtz solver (red line) and the analytical low-order code "OSCILOS" (black line).

4.2. Annular Combustion Chamber

The Helmholtz solver approach allows the nonlinear analysis on complex geometries that can be also characterized by the presence of multiple flames. In this section, the nonlinear behaviour of an annular combustor characterized by a plenum and an annular combustion chamber connected by a ring of twelve straight ducts (representing the burners) is analysed. The geometrical configuration is similar to the one introduced by Pankiewitz and Sattelmayer [39]. The mean diameter is 0.437 m, the external diameter of the plenum is 0.540 m and of the combustion chamber is 0.480 m. The length of the plenum is 0.200 m and of the combustion chamber is 0.300 m. Each burner has a diameter of 0.026 m and a length of 0.030 m. Temperature in the combustion chamber is 2.89 times the temperature on the plenum. Flame is assumed to be concentrated in a narrow zone at the entrance of the combus-

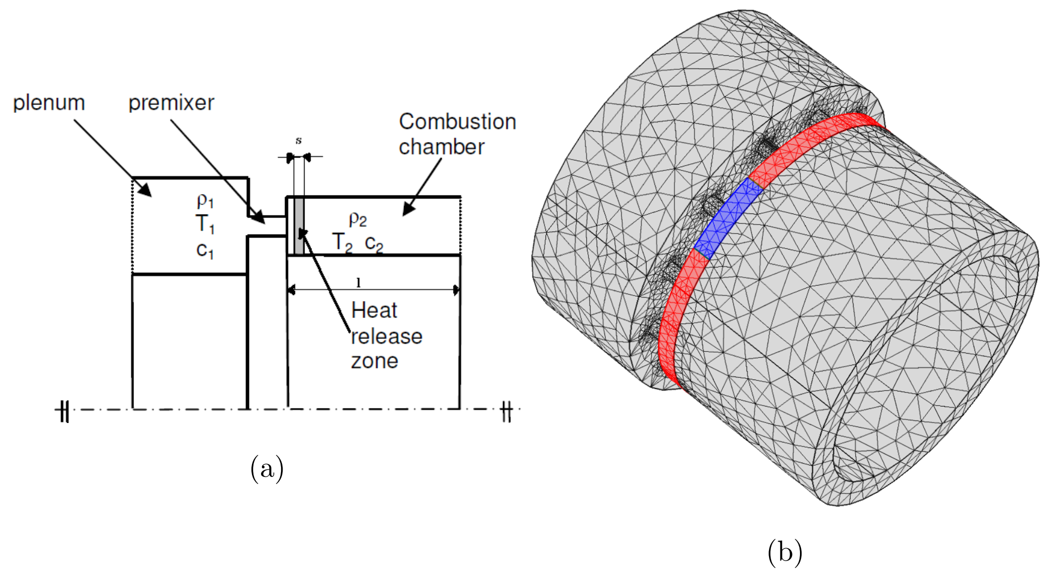

Figure 11: (a) Sketch of the annular combustion chamber. (b) Computational grid and flame zone highlighted in red. One of the twelve sectors, in which the flame zone is divided, is highlighted in blue.

tion chamber, as shown in Fig. 11, it is composed of twelve equal parts, one corresponding to each burner and, differently from what is done with other approaches [34, 35, 36] in each of them the flame model is defined. In so doing the heat release rate fluctuations are coupled to the velocity fluctuations of the corresponding burner, following the ISAAC (Independence Sector Assumption in Annular Combustors) assumption, introduced by Sensiau *et al.* [53]. This assumption states that *the heat release rate fluctuations in a given sector [of the combustion chamber] are only driven by the fluctuating mass flow rates due to the velocity perturbations through its own swirler.* Furthermore, following Wolf *et al.* [54] only the axial component of the velocity fluctuations is assumed to influence the flame dynamics. In the model, the reference point for the velocity fluctuations is considered in the middle of the burner, where the injection of the premixed mixture is usually located. In this work all burner are assumed to undergo the same velocity fluctuations level feature that is proper of a spinning mode [36]. Annular combustors can feature also standing and mixed azimuthal instabilities [14, 35] in which the burners operate with different amplitude of velocity fluctuations depending on the relative position with respect to the nodal line. Once the distribution of the velocity fluctuations is accounted, the numerical procedure to track the limit cycle conditions is identical to the one proposed in this article. In the analysed configuration, closed-end inlet and outlet are assumed as boundary conditions (u'=0). Losses due to viscous and thermal boundary layers are considered in the entire computational domain. In the plenum and in the combustion chamber a characteristic length ($\mathcal{L}$) of 0.212 m and 0.137 m, respectively, is used in the damping term of Eq. (11). Mean flow is neglected

Table 2: Frequencies of the first four modes of the annular combustor. Subscript "p" stands for plenum and "cc" for the combustion chamber

Mode Shape	(1,0,0)	(0,1_p,0)	(0,1_{cc},0)	(0,2,0)
Frequency Hz	309.4	446.5	734.8	839.3

also in this case. Table 2 shows the first four modes of the system without heat release rate fluctuations. Eigenmodes are denoted with the nomenclature (l, m, n), where l, m and n are, respectively, the orders of the pure axial, circumferential and radial modes.

For such configuration the most interesting mode is the first azimuthal

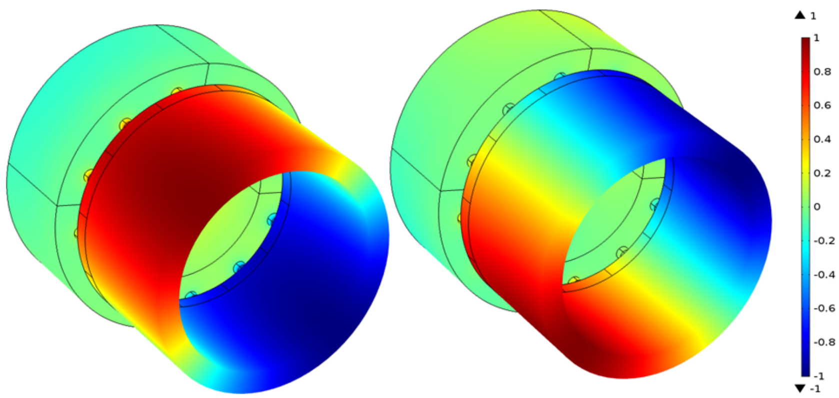

Figure 12: Wave shapes shifted of $\pi/2$ of the first azimuthal degenerate mode of the combustion chamber (mode (1,1,0) in Tab. 2) reported in terms of normalized acoustic pressure.

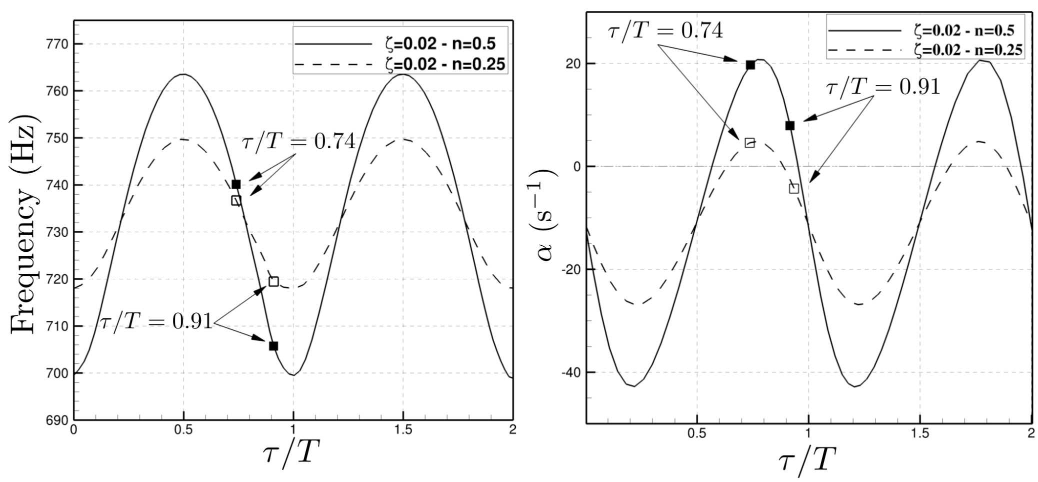

(a) (b)

Figure 13: Frequency (a) and growth rate (α) (b) of the azimuthal mode in the combustion chamber for $|\hat{u}/\overline{u}| \rightarrow 0$.

mode in the combustion chamber (mode (0,1$_{cc}$,0) in Tab. 2), since it is the most prone mode to experience instabilities in practical machines [40]. Figure 13 shows the results frequencies and growth rates of the linear stability analysis ($|\hat{u}/\overline{u}| \rightarrow 0$) considering a damping coefficient ζ=0.02 and two different values for the combustion-acoustic interaction index n. The time delay is varied from τ/T=0 to τ/T=2. In order to analyse the results of Fig. 13, following Lieuwen *et al.* [55], if the inlet section of the injector connected to a large plenum can be approximated as a pressure node, in the linear case without damping the regions of instability is predicted in bands where $C_k - 1/4 < \tau/T < C_k + 1/4$, being C_k=k-1/4 (k=1,2,...). In Fig. 13, due to the presence of the damping, results are different. With n=0.25, the mode is unstable only for 0.65< τ/T <0.9 and 1.65< τ/T <1.9 (dashed lines in Fig. 13). Increasing the interaction index results a shift towards more unstable conditions. Assuming an interaction index n=0.5 the regions of instabilities predicted by Lieuwen *et al.* [55] are obtained (solid lines in Fig. 13). So, in this configuration, the system passes from stable to unstable conditions for $\tau/T = k - 1/2$ (k=1,2,...), while from unstable to stable conditions for τ/T=k (k =1,2,...). It means that each of these conditions can be identified as bifurcation points in the nonlinear case. With the assumption of considering the same amplitude of velocity fluctuations for each burner the circumferential symmetry of the system is conserved. For each level of velocity fluctuations $|\hat{u}/\overline{u}|$, the eigenvalue analysis for the first azimuthal mode is degenerate. Combining the two mode structures shifted of $\pi/2$ shown in Fig. 12, a spinning mode is obtained [38]. Two conditions are taken into account: τ/T=0.74 and τ/T=0.91. The bifurcation diagrams for these two cases are tracked and shown in Fig. 14 considering both the flame models of Eq. (7) and Eq. (9). Again, a supercritical and a subcritical bifurcation occurs. The limit cycle for the two configurations occurs at different frequency which remain constant increasing of the control parameter: in the case of τ/T=0.74, it occurs at 735.9 Hz; in the case of τ/T=0.91, it occurs at 713.6 Hz. The influence of the time delay is again on the position of the Hopf point and fold point: a shift towards high value of n is observed with a higher τ/T is considered. In the subcritical bifurcation case, as for the longitudinal configuration, the amplitude of the fold point remains constant. Also in this configuration, the influence of the time delay decreases increasing the acoustic-combustion interaction index n. Both curves tends asymptotically to the value, which saturates the NFTF.

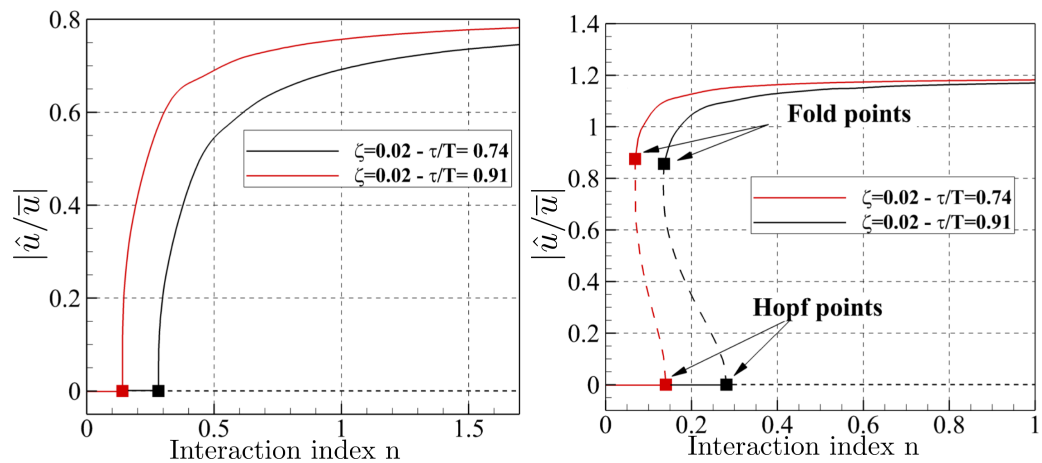

(a) (b)

Figure 14: Bifurcation diagrams of the first azimuthal mode in the combustion chamber of the annular combustion chamber in Fig. 11 with: (a) the nonlinear flame model of Eq. (9); (b) the nonlinear flame model of Eq. (7).

5. Conclusions

A numerical approach based on the use of the Helmholtz solver in order to study the limit cycles of longitudinal and azimuthal modes is presented in this article. The numerical procedure has been implemented in a FEM code able to treat any kind of three-dimensional geometries, with single and multiple burners. At first on a simple longitudinal combustor has been examined considering two nonlinear flame models consisting of a time delayed third-order polynomial and fifth-order polynomial saturation law. For this case, the bifurcation diagrams have been tracked evaluating the amplitude of the limit cycles at assuming the acoustic-combustion interaction index n as control variable. Two kinds of bifurcation have been found, depending on the nonlinear flame model. The third-order polynomial law features a supercritical bifurcation, whereas, the fifth-order polynomial nonlinear flame model features a subcritical bifurcation. The numerical approaches have been validating comparing the results against bifurcation diagrams obtained in the same configuration with an analytical tool. In a second step, an annular combustor equipped with twelve independent burners have been considered proving the ability of the proposed numerical technique to study the limit cycles occurring also in multiple flames configurations. The influence on the bifurcation of the time delay of the flame model and of the amount of damping considered in the system have been, subsequently, investigated in both configurations. As expected, increasing the damping coefficient, the amplitude of $|\hat{u}/\overline{u}|$ at limit cycles decreases. The time delay mainly influences the position of the Hopf bifurcation point and, in case of a subcritical bifurcation, of the fold point. On the contrary, the amplitude of the limit cycle at the fold point are not influenced by variations of the time delay. In both bifurcation behaviours at high values of the control parameter, the influence of the time delay and of the damping coefficient is low. The amplitude of limit cycles tends asymptotically to the value which nullifies the heat release rate fluctuations due to the saturation process induced by the nonlinear terms. The proposed approach proves to be able to treat nonlinear problems with simple configurations and, differently from other approaches described in the literature, more complex multi-burner configurations can be analysed making the described numerical approach to be also employed in an industrial environment. Numerical and experimental data can be introduced into the simulation model, performing parametric analyses which can be helpful both in the design and in the check stage of a burner.

Appendix 1: Nonlinear flame model derivation

Let consider the nonlinear flame model in Eq. (7) where the third-powered term is the highest order. The flame model is converted into the frequency domain assuming the flame response to a harmonic input

$$u'(t) = Re(\hat{u}e^{i\omega t}) = |\hat{u}| \cos(\omega t). \tag{16}$$

For finite disturbances, the flame model $\dot{q}'(t)$ may not be pure harmonic but is still periodic and hence it can be described by a Fourier series:

$$\dot{q}'(t) = Re\left(\sum_{m=0}^{\infty} \hat{\dot{q}}^m e^{im\omega t} \right), \tag{17}$$

where m is the order of the harmonics. Let now consider the first harmonic $\hat{\dot{q}}^{(1)}$. The nonlinear flame transfer function NFTF to be derived is a function of frequency and amplitude $|\hat{u}/\overline{u}|$. The first Fourier coefficient is written as

$$\hat{\dot{q}}^{(1)} = \frac{\omega}{\pi}\int_0^{2\pi/\omega} \dot{q}' e^{i\omega t} dt. \tag{18}$$

Introducing Eq. (16), Eq. (17) and the nonlinear flame model in Eq. (7), and considering the property of the Fourier transform that $F(u'(t-\tau)) = F(u'(t))e^{-i\omega\tau}$ it is shown that

$$\begin{aligned}\hat{\dot{q}}^{(1)} = \frac{\omega}{\pi}\int_0^{2\pi/\omega} -n\bar{\dot{q}}e^{-i\omega\tau}\left(\mu_2\left|\frac{\hat{u}}{\overline{u}}\right|^2\cos^2(\omega t)+\mu_0\right)\left|\frac{\hat{u}}{\overline{u}}\right|\cos(\omega t)\Bigg(\cos(\omega t)+\\ + i\sin(\omega t)\Bigg)dt = -n\bar{\dot{q}}\left|\frac{\hat{u}}{\overline{u}}\right|e^{-i\omega\tau}\left(\frac{\omega}{\pi}\int_0^{2\pi/\omega}\mu_2\cos^4(\omega t)\left|\frac{\hat{u}}{\overline{u}}\right|^2 dt+\right.\\ \left. + \frac{\omega}{\pi}\int_0^{2\pi/\omega}\mu_0\cos^2(\omega t)dt\right),\end{aligned} \tag{19}$$

where the imaginary term disappears because the integral from 0 to 2π of the product of cosine and sine is null. Additionally, it can be observed that even-powered polynomial terms are not mathematically admissible, because the cosine function is an even function and so the integral of its even-powered terms between 0 and 2π is null. Solving the integrals in Eq. (19) and considering that $\hat{\dot{q}}^L = -n\bar{\dot{q}}|\hat{u}/\overline{u}|e^{-i\omega\tau}$

$$\hat{\dot{q}}^{(1)} = \hat{\dot{q}}^L\left(\frac{3}{4}\mu_2\left|\frac{\hat{u}}{\overline{u}}\right|^2+\mu_0\right), \tag{20}$$

which is the nonlinear flame model $\mathcal{T}^{NL}_{flame}(\omega, |\hat{u}/\overline{u}|)$ of Eq. (6). Hence the function NFTF shown in Eq. (8) is obtained.

For the nonlinear flame model in Eq. (9) where the fifth-powered term is the highest order, considering the same assumption made for the first nonlinear flame model, the first Fourier coefficient for the second nonlinear flame model is written as

$$\hat{\dot{q}}^{(1)} = \frac{\omega}{\pi}\int_0^{2\pi/\omega} -n\bar{\dot{q}}e^{-i\omega\tau}\Bigg(\mu_4\left|\frac{\hat{u}}{\overline{u}}\right|^4\cos^4(\omega t) + \mu_2\left|\frac{\hat{u}}{\overline{u}}\right|^2\cos^2(\omega t) + \mu_0\Bigg)$$
$$\left|\frac{\hat{u}}{\overline{u}}\right|\cos(\omega t)\Bigg(\cos(\omega t) + i\sin(\omega t)\Bigg)dt = -n\bar{\dot{q}}\left|\frac{\hat{u}}{\overline{u}}\right|e^{-i\omega\tau}\Bigg(\frac{\omega}{\pi}\int_0^{2\pi/\omega}\mu_4$$
$$\cos^6(\omega t)\left|\frac{\hat{u}}{\overline{u}}\right|^4 dt + \frac{\omega}{\pi}\int_0^{2\pi/\omega}\mu_2\cos^4(\omega t)\left|\frac{\hat{u}}{\overline{u}}\right|^2 dt + \frac{\omega}{\pi}\int_0^{2\pi/\omega}\mu_0\cos^2(\omega t)dt\Bigg), \tag{21}$$

where the imaginary term disappears because the integral from 0 to 2π of the product of cosine and sine is null. Again, solving the integrals and considering that $\hat{\dot{q}}^L = -n\bar{\dot{q}}|\hat{u}/\overline{u}|e^{-i\omega\tau}$

$$\hat{\dot{q}}^{(1)} = \hat{\dot{q}}^L\left(\frac{5}{8}\mu_4\left|\frac{\hat{u}}{\overline{u}}\right|^4 + \frac{3}{4}\mu_2\left|\frac{\hat{u}}{\overline{u}}\right|^2 + \mu_0\right), \tag{22}$$

which is the (nonlinear) flame transfer function $\mathcal{T}^{NL}_{flame}(\omega, |\hat{u}/\overline{u}|)$ of Eq .(6). Hence the function NFTF shown in Eq. (8) is obtained.

References

[1] Fichera, A., Losenno, C., and Pagano, A., 2001. "Experimental analysis of thermo-acoustic combustion instability". *Applied Energy,* ***70***(2), pp. 179–191.

[2] Lieuwen, T. C., and Yang, V., 2005. "Combustion instabilities in gas turbine engines(operational experience, fundamental mechanisms and modeling)". *Progress in astronautics and aeronautics.*

[3] Fichera, A., and Pagano, A., 2006. "Application of neural dynamic optimization to combustion-instability control". *Applied energy,* ***83***(3), pp. 253–264.

[4] Zhao, D., and Li, L., 2015. "Effect of choked outlet on transient energy growth analysis of a thermoacoustic system". *Applied Energy,* ***160***, pp. 502 – 510.

[5] Subramanian, P., Sujith, R., and Wahi, P., 2013. "Subcritical bifurcation and bistability in thermoacoustic systems". *Journal of Fluid Mechanics,* ***715***, pp. 210–238.

[6] Juniper, M., 2012. "Triggering in thermoacoustics". *International Journal of Spray and Combustion Dynamics,* ***4***(3), pp. 217–238.

[7] Silva, C. F., Nicoud, F., Schuller, T., Durox, D., and Candel, S., 2013. "Combining a helmholtz solver with the flame describing function to assess combustion instability in a premixed swirled combustor". *Combustion and Flame,* ***160***(9), September, pp. 1743–1754.

[8] Zhang, Z., Zhao, D., Dobriyal, R., Zheng, Y., and Yang, W., 2015. "Theoretical and experimental investigation of thermoacoustics transfer function". *Applied Energy,* ***154***, pp. 131–142.

[9] Nicoud, F., Benoit, L., Sensiau, C., and Poinsot, T., 2007. "Acoustic modes in combustors with complex impedances and multidimensional active flames". *AIAA journal,* ***45***(2), pp. 426–441.

[10] Camporeale, S., Fortunato, B., and Campa, G., 2011. "A finite element method for three-dimensional analysis of thermoacoustic combustion instability". *Journal of Engineering for Gas Turbine and Power,* ***133***(1), p. 011506.

[11] Zhao, D., Li, S., Yang, W., and Zhang, Z., 2015. "Numerical investigation of the effect of distributed heat sources on heat-to-sound conversion in a t-shaped thermoacoustic system". *Applied Energy*, ***144***, pp. 204–213.

[12] Dowling, A., and Stow, S., 2003. "Acoustic analysis of gas turbine combustors". *Journal of Propulsion and Power*, ***19***(5), pp. 751–765.

[13] Dowling, A., 1997. "Nonlinear self-excited oscillations of a ducted flame". *Journal of Fluid Mechanics*, ***346***, pp. 271–290.

[14] Bauerheim, M., Nicoud, F., and Poinsot, T., 2016. "Progress in analytical methods to predict and control azimuthal combustion instability modes in annular chambers". *Physics of Fluids (1994-present)*, ***28***(2), p. 021303.

[15] Culick, F., 2006. *Unsteady Motions in Combustion Chambers for Propulsion Systems*. AGARD, AG-AVT-039.

[16] Ananthkrishnan, N., Deo, S., and Culick, F., 2005. "Reduced-order modeling and dynamics of nonlinear acoustic waves in a combustion chamber". *Combustion Science and Technology*, ***177***, pp. 1–27.

[17] Strogatz, S., 2001. *Nonlinear Dynamics and Chaos*. Westview Press.

[18] Moeck, J., Bothien, M., Schimek, S., Lacarelle, A., and Paschereit, C., 2008. "Subcritical thermoacoustic instabilities in a premixed combustor". *14th AIAA/CEAS Aeroacoustics Conference, 2946*.

[19] Jahnke, C., and Culick, F., 1994. "Application of dynamical systems theory to nonlinear combustion instabilities". *Journal of Propulsion and Power,* ***10***, pp. 508–517.

[20] Burnley, V., 1996. "Nonlinear Combustion Instabilities and Stochastic Sources". PhD Dissertation, California Inst. of Technology, Pasadena, USA.

[21] Juniper, M., 2011. "Triggering in the horizontal rijke tube: Non-normality, transient growth and bypass transition". *Journal of Fluid Mechanics,* ***667***, pp. 272–308.

[22] Subramanian, P., Mariappan, S., Sujith, R., and Wahi, P., 2010. "Bifurcation analysis of thermoacoustic instability in a horizontal rijke tube". *Int. Journal of Spray and Combustion Dynamics,* ***2***(4), pp. 325–356.

[23] Engelborghs, K., Luzyanina, T., and Roose, D., 2002. "Numerical bifurcation analysis of delay differential equations using dde-biftool". *ACM Transactions on Mathematical Software,* ***28***, pp. 1–21.

[24] Campa, G., and Juniper, M., 2012. "Obtaining bifurcation diagrams with a thermoacoustic network model". *ASME paper, GT2012-68241*.

[25] Dowling, A., 1999. "A kinematic model of a ducted flame". *Journal of Fluid Mechanics,* ***394***, pp. 51–72.

[26] Noiray, N., Durox, D., Schuller, T., and Candel, S., 2009. "A method for estimating the noise level of unstable combustion based on the flame describing function". *International Journal of Aeroacoustics,* ***8***, pp. 157–176.

[27] Boudy, F., Durox, D., Schuller, T., Jomaas, G., and Candel, S., 2011. "Describing function analysis of limit cycles in a multiple flame combustor". *Journal of Engineering for Gas Turbine and Power,* ***133***(6), p. 061502.

[28] Boudy, F., Durox, D., Schuller, T., and Candel, S., 2011. "Nonlinear mode triggering in a multiple flame combustor". *Proceedings of the Combustion Institute,* ***33***(1), pp. 1121–1128.

[29] Palies, P., Durox, D., Schuller, T., and Candel, S., 2011. "Nonlinear combustion instability analysis based on the flame describing function applied to turbulent premixed swirling flames". *Combustion and Flame,* ***158***(10), pp. 1980–1991.

[30] Illingworth, S., Waugh, I., and Juniper, M., 2013. "Finding thermoacoustic limit cycles for a ducted burke-schumann flame". *Proceedings of the Combustion Institute,* ***34***(1), pp. 911–920.

[31] Kabiraj, L., Sujith, R., and Wahi, P., 2012. "Bifurcations of self-excited ducted laminar premixed flames". *Journal of Engineering for Gas Turbine and Power,* ***134***(3), p. 031502.

[32] Heckl, M., 2013. "Analytical model of nonlinear thermo-acoustic effects in a matrix burner". *Journal of Sound and Vibration,* ***332***, pp. 4021–4036.

[33] Noiray, N., Bothien, M., and Schuermans, B., 2011. "Investigation of azimuthal staging concepts in annular gas turbines". *Combustion Theory and Modelling,* ***15***(5), pp. 585–606.

[34] Ghirardo, G., and Juniper, M. P., 2013. “Azimuthal instabilities in annular combustors: standing and spinning modes”. *Proceedings of the Royal Society of London A: Mathematical, Physical and Engineering Sciences,* ***469***(2157), p. 20130232.

[35] Noiray, N., and Schuermans, B., 2013. “On the dynamic nature of azimuthal thermoacoustic modes in annular gas turbine combustion chambers”. In Proceedings of the Royal Society of London A: Mathematical, Physical and Engineering Sciences, Vol. 469, The Royal Society, p. 20120535.

[36] Bourgouin, J.-F., Durox, D., Moeck, J. P., Schuller, T., and Candel, S., 2015. “Characterization and modeling of a spinning thermoacoustic instability in an annular combustor equipped with multiple matrix injectors”. *Journal of Engineering for Gas Turbines and Power,* ***137***(2), p. 021503.

[37] Parmentier, J.-F., Salas, P., Wolf, P., Staffelbach, G., Nicoud, F., and Poinsot, T., 2012. “A simple analytical model to study and control azimuthal instabilities in annular combustion chambers”. *Combustion and Flame,* ***159***(7), pp. 2374–2387.

[38] Bauerheim, M., Parmentier, J.-F., Salas, P., Nicoud, F., and Poinsot, T., 2014. “An analytical model for azimuthal thermoacoustic modes in an annular chamber fed by an annular plenum”. *Combustion and Flame,* ***161***(5), pp. 1374–1389.

[39] Pankiewitz, C., and Sattelmayer, T., 2003. “Time domain simulation of

combustion instabilities in annular combustors". *Journal of Engineering for Gas Turbine and Power,* ***125***(2), pp. 677–685.

[40] Campa, G., and Camporeale, S. M., 2014. "Prediction of the thermoacoustic combustion instabilities in practical annular combustors". *Journal of Engineering for Gas Turbines and Power,* ***136***(9), p. 091504.

[41] Staffelbach, G., Gicquel, L., Boudier, G., and Poinsot, T., 2009. "Large eddy simulation of self excited azimuthal modes in annular combustors". *Proceedings of the Combustion Institute,* ***32***(2), pp. 2909 – 2916.

[42] Wolf, P., Balakrishnan, R., Staffelbach, G., Gicquel, L. Y., and Poinsot, T., 2012. "Using les to study reacting flows and instabilities in annular combustion chambers". *Flow, Turbulence and Combustion,* ***88***(1-2), pp. 191–206.

[43] Poinsot, T., and Veynante, D., 2001. *Theoretical and Numerical Combustion.* R. T. Edwards Incorporated.

[44] Munjal, M., 1986. *Acoustics of Ducts and Mufflers.* John Wiley & Sons.

[45] Matveev, K., 2003. "Thermoacoustic instabilities in the rijke tube: experiments and modeling". PhD thesis, California Institute of Technology.

[46] Crocco, L., and Cheng, S.-I., 1956. *Theory of combustion instability in liquid propellant rocket motors.* Cambridge Univ Press.

[47] Goh, C. S., and Morgans, A. S., 2013. "The influence of entropy waves

on the thermoacoustic stability of a model combustor". *Combustion Science and Technology,* ***185***(2), pp. 249–268.

[48] Durox, D., Schuller, T., Noiray, N., and Candel, S., 2009. "Experimental analysis of nonlinear flame transfer functions for different flame geometries". *Proceedings of the Combustion Institute,* ***32***(1), pp. 1391 – 1398.

[49] Stow, S. R., and Dowling, A. P., 2009. "A time-domain network model for nonlinear thermoacoustic oscillations". *Journal of engineering for gas turbines and power,* ***131***(3), p. 031502.

[50] Lehoucq, R. B., Sorensen, D. C., and Yang, C., 1998. *ARPACK users' guide: solution of large-scale eigenvalue problems with implicitly restarted Arnoldi methods*, Vol. 6. Siam.

[51] Schuller, T., 2003. "Mécanismes de Couplage dans les Interactions Acoustique-Combustion". Ph.D. Thesis, Ecole Central paris.

[52] Li, J., and Morgans, A. S., 2015. "Time domain simulations of nonlinear thermoacoustic behaviour in a simple combustor using a wave-based approach". *Journal of Sound and Vibration,* ***346***, pp. 345 – 360.

[53] Sensiau, C., Nicoud, F., and Poinsot, T., 2008. "Thermoacoustic analysis of an helicopter combustion chamber". *AIAA paper, AIAA-2008-2947*.

[54] Wolf, P., Staffelbach, G., Gicquel, L. Y., Müller, J.-D., and Poinsot, T., 2012. "Acoustic and large eddy simulation studies of azimuthal modes

in annular combustion chambers". *Combustion and Flame,* ***159***(11), pp. 3398–3413.

[55] Lieuwen, T., Torres, H., Johnson, C., and Zinn, B. T., 2001. "A mechanism of combustion instability in lean premixed gas turbine combustors". *Journal of Engineering for Gas Turbines and Power,* ***123***(1), pp. 182–189.